Published in "Development 137: 2187-2196 , 2010"
which should be cited to refer to this work.

Pulsatile shear and Gja5 modulate arterial identity and remodeling events during flow-driven arteriogenesis

Ivo Buschmann[1,2,10,*], Axel Pries[3,*], Beata Styp-Rekowska[3], Philipp Hillmeister[1,10], Laurent Loufrani[4], Daniel Henrion[4], Yu Shi[1], Andre Duelsner[1], Imo Hoefer[5], Nora Gatzke[1], Haitao Wang[1], Kerstin Lehmann[1], Lena Ulm[3], Zully Ritter[6], Peter Hauff[7], Ruslan Hlushchuk[8], Valentin Djonov[8], Toon van Veen[9] and Ferdinand le Noble[1,10,11,†]

SUMMARY

In the developing chicken embryo yolk sac vasculature, the expression of arterial identity genes requires arterial hemodynamic conditions. We hypothesize that arterial flow must provide a unique signal that is relevant for supporting arterial identity gene expression and is absent in veins. We analyzed factors related to flow, pressure and oxygenation in the chicken embryo vitelline vasculature in vivo. The best discrimination between arteries and veins was obtained by calculating the maximal pulsatile increase in shear rate relative to the time-averaged shear rate in the same vessel: the relative pulse slope index (RPSI). RPSI was significantly higher in arteries than veins. Arterial endothelial cells exposed to pulsatile shear in vitro augmented arterial marker expression as compared with exposure to constant shear. The expression of Gja5 correlated with arterial flow patterns: the redistribution of arterial flow provoked by vitelline artery ligation resulted in flow-driven collateral arterial network formation and was associated with increased expression of Gja5. In situ hybridization in normal and ligation embryos confirmed that *Gja5* expression is confined to arteries and regulated by flow. In mice, Gja5 (connexin 40) was also expressed in arteries. In the adult, increased flow drives arteriogenesis and the formation of collateral arterial networks in peripheral occlusive diseases. Genetic ablation of Gja5 function in mice resulted in reduced arteriogenesis in two occlusion models. We conclude that pulsatile shear patterns may be central for supporting arterial identity, and that arterial Gja5 expression plays a functional role in flow-driven arteriogenesis.

KEY WORDS: Gja5 (connexin 40), Arterial-venous differentiation, Arteriogenesis, Blood flow, Pulsatile shear, Chick, Mouse

INTRODUCTION

Arterial and venous vascular networks show a distinct genetic signature, function and branching architecture (De Smet et al., 2009; Swift and Weinstein, 2009). Specification of arterial-venous vessel identity and the formation of branched vascular networks occur during early embryogenesis and are modulated by hemodynamic factors (Jones et al., 2004; le Noble et al., 2004; Lucitti et al., 2007), but the precise mechanisms are unclear. Circulation of blood creates mechanical forces in vessels (Garcia-Cardena et al., 2001; Jones et al., 2006) and affects oxygenation of developing organs. Here, we investigated which mechanical forces, or secondary factors including oxygenation of the blood (Fraisl et al., 2009), might be relevant for regulating vessel identity in developing embryonic vascular networks in vivo. We furthermore assessed the morphological and genetic changes that occur in the embryonic yolk sac vasculature in response to manipulations of hemodynamic conditions, and show that genes strongly expressed therein might also exert a functional role in collateral arterial network growth (Buschmann and Schaper, 1999; Schaper, 2009) during pathological conditions.

In the embryo, vascular branching morphogenesis and vessel identity can be regulated by two distinct mechanisms: genetic hardwiring of vessel positioning and identity, and hemodynamics-controlled vascular patterning and identity regulation (Jones et al., 2006). Hardwiring of vessel positioning at the capillary level involves endothelial tip cells and occurs independently of blood flow (Gerhardt et al., 2003; Hellstrom et al., 2007; Ruhrberg et al., 2002; Stalmans et al., 2002). Arterial specification requires activation of sonic hedgehog/VEGF/neuropilin 1/Notch pathways (Lawson et al., 2001; Lawson et al., 2002; Swift and Weinstein, 2009; Zhong et al., 2001). Venous specification involves chicken ovalbumin upstream promoter-transcription factor II (COUP-TFII; also known as Nr2f2) (You et al., 2005), which acts as a repressor of arterial specification signaling. At present, neuropilin 1 (Herzog et al., 2001; Moyon et al., 2001), ephrin B2 (Adams et al., 1999; Gerety and Anderson, 2002; Wang et al., 1998), Unc5b (Lu, 2004), Notch1, Notch4, Jag1, Jag2 and Dll4 (Duarte et al., 2004; Krebs et al., 2004; Krebs et al., 2000; Shutter et al., 2000; Villa et al., 2001) are established arterial markers, whereas EphB4 (Adams et al., 1999; Gerety et al., 1999; Wang et al., 1998), neuropilin 2 (Herzog et al., 2001; Yuan et al., 2002) and COUP-TFII (You et al., 2005)

[1]Experimental and Clinical Research Center (ECRC) of the Charite and the Max-Delbrueck Center for Molecular Medicine (MDC), D13125 Berlin-Buch, Germany. [2]Department of Internal Medicine/Cardiology, CCR, Charite, D10115 Berlin, Germany. [3]Department of Physiology, CCR and German Heart Center, Charite, D14195 Berlin, Germany. [4]Department of Neurovascular Biology, UMR 6214 Inserm U771, University of Angers, 49045 Angers, France. [5]Department of Experimental Cardiology, Division of Heart & Lungs, UMC, 3584 CM Utrecht, The Netherlands. [6]Department of Radiology, CBF, Charite, D12203 Berlin, Germany. [7]Bayer Schering Pharma AG, MicroCT Unit, D13353 Berlin, Germany. [8]Department of Gross Anatomy and Vascular Biology, University of Fribourg, CH1700 Fribourg, Switzerland. [9]Department of Medical Physiology, Division of Heart & Lungs, UMC, 3585 CH Utrecht, The Netherlands. [10]Center for Stroke Research Berlin (CSB), Charite, D10117 Berlin, Germany. [11]Max-Delbrueck Center for Molecular Medicine (MDC), Department of Angiogenesis and Cardiovascular Pathology, D13125 Berlin, Germany.

*These authors contributed equally to this work
[†]Author for correspondence (lenoble@mdc-berlin.de)

mark veins. In the mouse (Jones et al., 2008; Lucitti et al., 2007) and chicken embryo yolk sac vasculature, hemodynamic factors contribute to arterial-venous differentiation, which involves the regulation of arterial marker expression (le Noble et al., 2004). In the adult, hemodynamic factors regulate the enlargement and outgrowth of collateral arterial networks upon arterial occlusion (Carmeliet, 2000; Eitenmuller et al., 2006). Several molecules originally described in embryonic arterial remodeling also modulate the efficiency of arterial collateralization in the adult (Limbourg et al., 2007; Takeshita et al., 2007).

Besides these classical morphogenes, arteries also express the gap junction proteins Gja4 (connexin 37) and Gja5 (connexin 40) (Gustafsson et al., 2003; Haefliger et al., 2004; Mukouyama et al., 2002; Simon and McWhorter, 2002). Gap junction proteins mediate the direct diffusion of signals between adjacent cells (Wagner, 2008). In the microcirculation, gap junction proteins facilitate electrical coupling between endothelial cells (Schmidt et al., 2008), which plays an important role in the regulation of vascular tone (de Wit et al., 2000; Hill et al., 2002). The mechanism underlying arterial-specific regulation of connexins remains unknown.

We hypothesized that arterial flow must generate a unique signal that is relevant for driving arterial identity gene expression and is absent from veins. We considered factors related to flow, pressure and oxygenation and found a unique parameter related to the pulsatility of blood flow that distinguishes arterial from venous domains: the relative pulse slope index (RPSI). We identified strong expression of Gja5 during flow-driven arterial remodeling events in the embryo, and obtained genetic evidence in mice showing the functional importance of Gja5 in flow-driven arterial remodeling and collateral arterial network development.

MATERIALS AND METHODS

Chick embryos

Fertilized chicken eggs (*Gallus gallus*, White Leghorn) were purchased from commercial sources and incubated at 38°C in a humidified atmosphere. Embryo stages were determined according to the number of somites formed. Handling of the embryos and ligation of the right vitelline artery were performed as described (le Noble et al., 2004). FITC-dextran (Sigma, 200 kDa; 8 mg/ml in PBS), used to visualize plasma flow, was injected intravascularly using a micropipette. Scanning electron microscopy of vascular casts was performed as described (le Noble et al., 2004).

In vivo microscopy, time-lapse imaging and measurement of red blood cell velocity and oxygen saturation in vivo

In vivo time-lapse imaging and intravital video-microscopy were performed as described (le Noble et al., 2004). Briefly, yolk sac blood vessels were imaged using a 25× objective (NA 0.6) and asynchronous strobe light illumination (Lindert et al., 2002; Pries et al., 1994). This illumination generates image pairs with a time delay (Δt) of as little as 0.5 milliseconds. In the off-line analysis, a line is defined along the center of the vessel, and the light intensity pattern along this line, which is generated by the red blood cell column, is recorded for each image pair. Using a correlation algorithm, the spatial displacement (Δl) of the intensity pattern during Δt is determined. The center-line flow velocity (v) is then calculated as $v=\Delta l/\Delta t$, with a temporal resolution of 25 Hz and a maximal measurable velocity of 40 mm/second. Individual velocity values obtained over three to five heart cycles were averaged to obtain the mean flow velocity for a given vessel. Shear rate values were estimated by dividing the flow velocity by vessel diameter (d). For determination of oxygen saturation, a multispectral approach was used (Styp-Rekowska et al., 2007).

In situ hybridization

In toto in situ hybridization using antisense mRNA probes for chicken *Gja5* (ENSGALT00000024975) (Takebayashi-Suzuki et al., 2000) and *COUP-TFII* was performed as described (le Noble et al., 2004). For *COUP-TFII* (*Nr2f2*, Ensembl transcription ID: ENSGALT00000023630), we cloned an 806 bp fragment comprising bp 61 to 867 of the open reading frame. Note that *Gja5* encodes connexin 40 in mammals and connexin 42 in chicken; for clarity, we refer to Gja5.

In vitro experiments in endothelial cells

Human endothelial cells (HUAEC and HUVEC, PromoCell, Heidelberg, Germany) were cultured to 90% confluency at 37°C and 5% CO_2. Endothelial cells were subjected to shear stress in a modified cone-and-plate viscometer. Cells were exposed to 1-30 dyne/cm^2 pulsatile laminar shear stress with a frequency of 1 Hz, or constant shear stress (30 dyne/cm^2), or no stress as a static control (0 dyne/cm^2). Dextran T-70 (Sigma), at 5% in cell culture medium, was added to the cell culture medium to increase the viscosity 2.95-fold to 0.02065 dyne/second/cm^2. After the application of shear stress for 24 hours, cells were washed twice in PBS. Total RNA was isolated using TRIzol (Invitrogen). Real-time RT-PCR was performed using TaqMan (Applied Biosystems) probe-based chemistry. Primers and probes (BioTez, Berlin, Germany) were designed using Primer Express 2.0 software (Applied Biosystems) (Table 1). The real-time PCR amplification reaction was performed on a Sequence Detection System (7900 HT, Applied Biosystems) using the TaqMan Gene Expression MasterMix according to the manufacturer's instructions. Reactions were performed in triplicate. Data were collected and analyzed with Sequence Detection System 2.3 software. The relative amount of mRNA was calculated after normalization to *Gapdh*.

Mouse strains

Connexin 40 mutant (*Gja5*$^{-/-}$), connexin 40 floxed (*Gja5*$^{flox/flox}$), tamoxifen-inducible *Tie2 Cre* (*Tie2CreERT2*) and connexin 40-GFP reporter mice were as described (Chadjichristos et al., 2010; Forde et al., 2002; Miquerol et al., 2004; Simon et al., 1998). To generate tamoxifen-inducible endothelial cell-specific *Gja5* mutant mice, we mated the *Tie2CreERT2* transgenic mice with *Gja5*$^{flox/flox}$ mice. For induction of Cre

Table 1. Primer and probe sequences (5′ to 3′) for the real-time PCR

Gene	Forward primer	Reverse primer	TaqMan probe†
GAPDH	GAAGGTGAAGGTCGGAGTC	GAAGATGGTGATGGGATTTC	CAAGCTTCCCGTTCTCAGCC
DLL1	CTGCCTGCCTGGATGTGAT	AGACAGCCTGGATAGCGGATAC	TACCGGCCCTGCCAGCCCA
DLL4	CCAGGAAAGTTTCCCCACAGT	CCGACACTCTGGCTTTTCACT	GTAACCGCAGTGGCGCCTTCTCT
EFNB2	TCTTCCTCATTGCTGTGGTTGT	CTTGTCCGTGTACTCCGAGTCA	ATCGCCATCGTGTGTAACAGACGG
HES1	GGACATTCTGGAAATGACAGTGAA	CAGCGCAGCCGTCATCT	CGCCCGCTGCAGGTTCCG
HEY1	TGACCGTGGATCACCTGAAA	GCGTGCGCGTCAAAGTAAC	TGCTGCATACGGCAGGAGGGAAA
HEY2	CAAGAAAGAAAAGGAGAGGGATTATAGA	TTGGCACAAGTCTTCTCAACTCA	AAAGGCGTCGGGATCGGATAAATAACAGTT
NRP1	TGTGAAGTGGAAGCCCCTACA	CCTGGTCGTCATCACATTCATC	ACCGACCACTCCCAACGGGAACTT
GJA5	CACCACCCCCCGACTTTAA	CATATTATTGCTGAAGGGATTGAAGA	TGCCTGGAGAATGGCCCTGGG
COUP-TFII	CCATAGTCCTGTTCACCTCAGATG	CCTAACGTATTCTTCCAAAGCACACT	TGTGGTCTCTCTGATGTAGCCCAT
*Gapdh**	GGCAAATTCAACGGCACAGT	AGATGGTGATGGGCTTCCC	AGGCCGAGAATGGGAAGCTTGTCATC
*Gja5**	CAGCCTGGCTGAACTCTACCA	CTGCCGTGACTTGCCAAAG	CGCTGTCGGATCTTCTTCCAGCCCAG

*Mouse genes; the remainder are human.
†Probes have 5′ FAM and 3′ TAMRA labels.

activity, *Gja5*$^{flox/flox}$ mice carrying the *Tie2CreERT2* transgene (Tc^{+}), as well as their Cre-negative (Tc^{-}) littermates, were injected intraperitoneally with tamoxifen (30 mg/kg body weight) once a day for a period of 2 weeks, prior to performing artery occlusion. The primers used for genotyping the conditional *Gja5* mutant mice are listed in Table S1 in the supplementary material.

Femoral artery occlusion model and assessment of blood flow with LDF

Occlusion of the right femoral artery in 12-week-old mice was performed as described (Hoefer et al., 2004) (see Fig. S7 in the supplementary material). For repetitive assessment of hindlimb blood flow after occlusion, we used the non-invasive laser Doppler (LDF) imaging technique (Chalothorn et al., 2005). The LDF technique depends on the Doppler principle, whereby low-power light from a monochromatic stable laser (830 nm, laser diode, model LDI2-HR, Moor Instruments, Millwey, Axminster, UK) incident on tissue is scattered by moving red blood cells and is photo-detected and processed to provide a blood flow measurement. The term used to describe blood flow measured by the LDF technique is 'flux', a quantity that is proportional to the product of the average speed of the blood cells and the blood volume. This is expressed in arbitrary 'perfusion units' and is calculated using the first moment of the power spectral density. In our figures, we indicate 'perfusion units'.

MicroCT imaging

For visualization of the arterial collateral network after femoral artery occlusion, we used microCT imaging. Briefly, 7 days after femoral artery occlusion, the abdominal aorta was cannulated and perfused with 100 mg/kg body weight papaverin hydrochloride (Paveron, Weimer, Germany) to obtain maximal vasodilation, followed by perfusion with Microfil (MV-122, Flow Tech, Carver, MC, USA). Collateral arterial network morphology was analyzed with Amira 5.2.2 software (Visage Imaging, Berlin, Germany) after PET/CT (Inveon, Siemens) scanning with a resolution of 20 µm. All measurements were taken directly from the three-dimensional reconstruction.

Mouse mesenteric ligation model

To study the effects of a chronic increase in blood flow on outward remodeling in the arteries of mice, we used the mesenteric ligation model as described (Loufrani et al., 2002) (see Fig. S8 in the supplementary material). Cannulated arterial segments were bathed in a 5 ml organ bath of a Ca^{2+}-free physiological salt solution containing 2 mM EGTA and 10 µM sodium nitroprusside (to obtain maximal vasodilation). Pressure steps (10-150 mm Hg) were then performed to determine passive arterial diameter. Pressure and diameter measurements were collected using a Biopac Data Acquisition System (MP100 and AcqKnowledge software, Biopac, La Jolla, CA, USA). The care and euthanasia of mice were in accordance with European Community Standards on the Care and Use of Laboratory Animals (Ministère de l'Agriculture, France), and the protocol was approved by the local ethical committee.

Statistical analysis

Data are expressed as mean ± s.e.m. *P*-values were calculated (SigmaStat v3, Systat software) using Student's *t*-test, Mann Whitney U-test (for non-normal distributions), *z*-test for comparison of proportions, or two-way analysis of variance (pressure-diameter curves). $P<0.05$ was considered statistically significant.

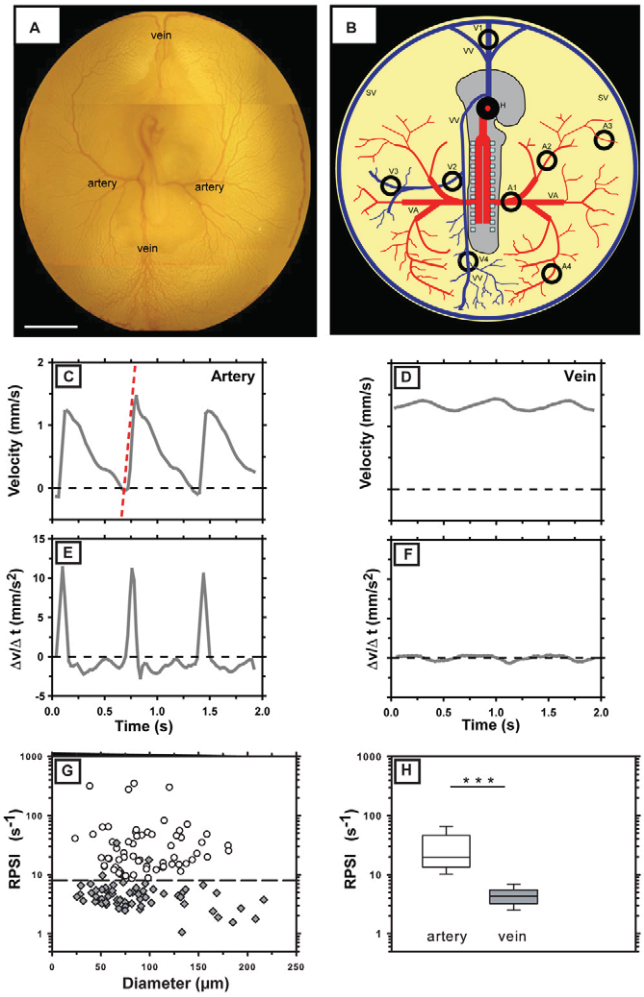

Fig. 1. In vivo measurements of red blood cell velocities in yolk sac arteries and veins. (**A**) Overview of the chicken embryo yolk sac vascular network in vivo. (**B**) Schematic representation of the vascular plexus. Arteries are indicated in red, veins in blue. A1-A4 indicate the measurement sites (circled) in arteries, V1-V4 in veins. (**C-F**) Red blood cell velocity profiles (C,D) and the corresponding first-order derivative of velocity, i.e. acceleration rate (Δv/Δt) (E,F), in arteries and veins. The vertical dashed line in C indicates the first-order derivative for the time point of fastest acceleration (peak velocity increase, PVI). (**G**) Maximal acceleration rate normalized to mean velocity (relative pulse slope index, RPSI) as a function of diameter yields a separation of arterial (top, circles) and venous (bottom, squares) domains. Optimal separation of arterial from venous vessels occurs at a cut-off of RPSI=7.9 second^{-1}. (**H**) RPSI is significantly higher in arteries than veins. ***, $P<0.001$, Mann Whitney U-test. H, heart; VA, vitelline artery; VV, vitelline vein; SV, sinus vein. Scale bar: 3 mm.

RESULTS

In vivo imaging of blood flow parameters and oxygen in chicken embryo arteries and veins

Adaptation to shear stress and identification of relative pulse slope index (RPSI) as a parameter to discriminate arteries from veins

Red blood cell velocity (vRBC) was measured in arteries and veins in vivo (Fig. 1A,B). Arteries showed a high pulsatility in the flow velocity profile (Fig. 1C), compared with the more constant flow velocity in veins (Fig. 1D). From the velocity profiles we calculated the red blood cell acceleration rate (first-order derivative, Δv/Δt, in mm/second^2, see red line in Fig. 1C) during each heart cycle. Note the steep acceleration rates during the initial systole in arteries (Fig. 1E), but not in veins (Fig. 1F). Mean shear rate was calculated from mean velocity/vessel diameter; mean velocity was determined from the velocity profile averaged from three to five heart cycles. For arteries, we analyzed 65 vessels (diameter range of 24-180 µm) from ten embryos at the 30- to 33-somite stage (ss). For veins we analyzed 60 vessels (diameter range of 20-225 µm) from ten embryos at 30-33 ss. We next examined which flow-

related parameter discriminates arteries from veins (Fig. 1G,H; see Figs S1, S2 in the supplementary material). Mean velocity, mean shear rate and maximal red blood cell acceleration rate ($\Delta v/\Delta t$ max), as a function of vessel diameter, did not sufficiently discriminate arteries from veins (see Fig. S1A-C in the supplementary material). However, the maximal acceleration rate of the red blood cells (as occurs during early systole) varied systematically as a function of the mean velocity in that vessel (see Fig. S1D in the supplementary material). It was possible to achieve an almost complete separation of the arterial and venous domains by a line with a slope of 1 and a relation of maximal acceleration to mean velocity of 7.9.

This observation suggested that the quotient maximal acceleration/mean velocity is suited to discriminate arteries from veins (Fig. 1G,H). The resulting parameter is referred to as the relative pulse slope index (RPSI): the maximal acceleration rate/mean vRBC second^{-1}. Considering the proportionality between shear and flow velocity for a given vessel diameter, RPSI is identical to the maximal positive change in shear rate relative to the time-averaged shear rate in the same vessel. RPSI was significantly higher in arteries than veins, with almost no overlap between the two domains at a cut-off of 7.9 second^{-1} (Fig. 1G,H; see Fig. S2 in the supplementary material, ROC analysis). Arteries have RPSI values exceeding 7.9 with 99% confidence. Comparable results were obtained in 22 ss and 44 ss embryos (see Fig. S3 in the supplementary material).

Cyclic stretch is limited to the aorta

As a result of the rhythmic activity of the heart, arterial pressure fluctuates. In the adult, the distensible nature of the arteries averages out the pressure pulsations, which involves cyclic stretching of the arteries. Arterial pressures in the yolk sac vasculature are extremely low and range from 0.4 mm Hg (HH stage 14) to ~1.35-0.8 mm Hg (HH stage 23) (Girard, 1973; Van Mierop and Bertuch, 1967). We observed a small, but significant, degree of cyclic stretch (2.93±0.57%, n=23) in the aorta. In vitelline arteries and venules, distension was not detectable in all animals investigated (n=15 animals, five to six arteries or veins per animal). The lack of distensibility supports pulsatile flow up to the distal parts of the yolk sac arterioles.

Oxygen measurements in arteries and veins and hypoxia challenge in vivo

In line with the yolk sac functioning as a placenta, we observed significantly lower (P<0.001) oxygen saturation levels in arteries than veins (63.2±1.9% versus 78.4±3%, n=6; see Fig. S4A in the supplementary material). Exposing chicken embryos to hypoxia (an ambient oxygen level of 10%) induced cardiac malformations (7/8 embryos) and a smaller and less well-branched arterial network than in normoxic controls (see Fig. S4B in the supplementary material).

Effects of constant and pulsatile shear on the expression of arterial identity genes

To substantiate that pulsatility influences the expression of arterial markers, we used an in vitro approach (Fig. 2). Human arterial endothelial cells (HUAEC) were exposed to pulsatile or constant shear and analyzed for the expression of eight arterial markers: delta-like 1 (*DLL1*), delta-like 4 (*DLL4*), *HEY1*, *HEY2*, *HES1*, ephrin B2 (*EFNB2*), neuropilin 1 (*NRP1*) and *GJA5* (Fig. 2A-H). The expression of all these arterial markers was augmented in the presence of pulsatile shear when compared with constant shear.

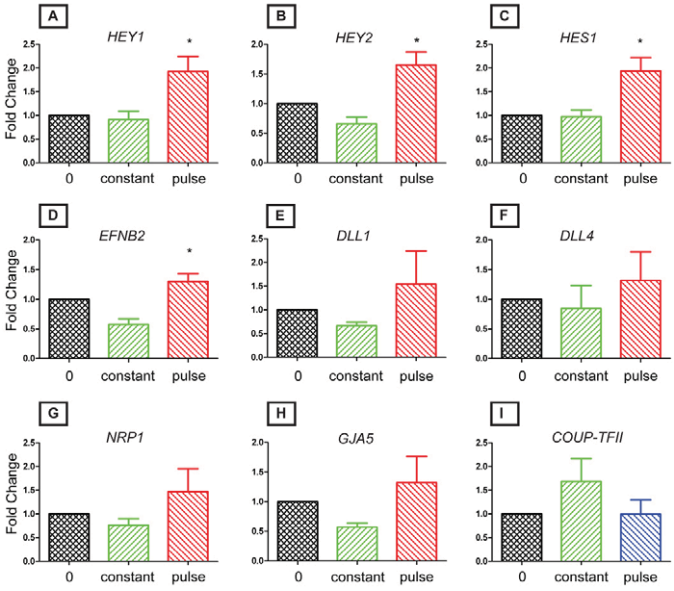

Fig. 2. Effects of pulsatile and constant shear on marker gene expression in vitro. (**A-H**) Effects of constant and pulsatile shear (pulse) on mRNA expression of the arterial markers (A) *HEY1*, (B) *HEY2*, (C) *HES1*, (D) ephrin B2 (*EFNB2*), (E) delta-like 1 (*DLL1*), (F) delta-like 4 (*DLL4*), (G) neuropilin 1 (*NRP1*) and (H) *GJA5*, as measured in human arterial endothelial cells. (**I**) Expression of the venous marker COUP-TFII in venous endothelial cells. n=4 separate experiments; *, P<0.05, versus exposure to constant shear stress.

This response was particularly clear for the Notch downstream signaling molecules *HEY1*, *HEY2*, *HES1* and *EFNB2* (Fig. 2A-D). COUP-TFII acts as a master regulator of venous identity by repressing the expression of arterial markers (Swift and Weinstein, 2009; You et al., 2005). In our arterial endothelial cells, COUP-TFII was expressed only marginally when compared with expression in venous endothelium, and COUP-TFII expression in arterial endothelium was not altered by constant or pulsatile shear (data not shown). We therefore evaluated COUP-TFII expression in venous endothelial cells (HUVEC) (Fig. 2I). Venous endothelial cells exposed to constant shear stress augmented COUP-TF-II expression, which was not observed after exposure to pulsatile shear (Fig. 2I).

Flow-driven macroscopic and microscopic changes in the arterial network

We next investigated arterial adaptation in response to changes in flow using the chicken embryo ligation model. We first quantified the flow changes that occur in the proximal and distal parts of the left vitelline artery (LVA) after ligation of the right vitelline artery (RVA) (Fig. 3A,B); measurements were made in the same vessel pre- and post-ligation (n=12). Mean velocities and mean shear rates increased significantly in both the proximal and distal areas (Fig. 3C-F). We observed no acute diameter change in these arteries. Thus, ligation of the RVA increased perfusion of the LVA arterial network up to the most distal branches.

Ligation of the RVA resulted in pruning of the arterial segment proximal to the ligation and outward remodeling of the comparable arterial segment on the contralateral side (Fig. 3G-L). At 5 hours post-ligation, lumen diameters of the stem of the RVA were significantly smaller (P<0.001, n=6; Fig. 3G,H,L), and after 24 hours the right arterial segment was anatomically undetectable in

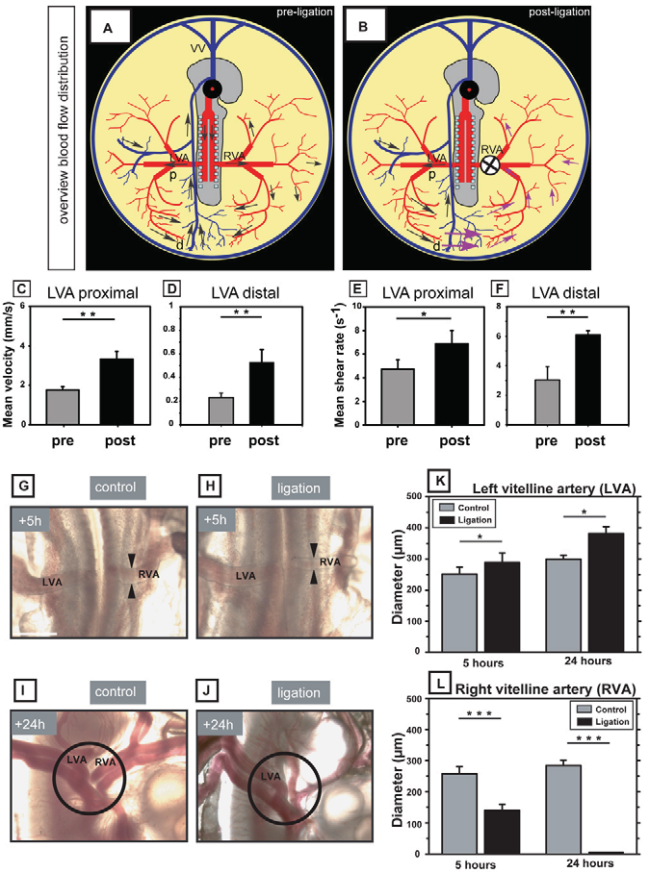

Fig. 3. Flow redistribution and diameter adaptation in the ligation model. (**A**,**B**) Flow distribution in the chicken embryo yolk sac posterior pole before (A) and after (B) ligation of the right vitelline artery (RVA). Note the reversed flow direction in RVA distal arterioles. Black arrows indicate normal flow direction, purple arrows the changed directions. (**C-F**) In proximal and distal arterioles of the left vitelline artery (LVA), mean velocities (C,D) and mean shear rates (E,F) increase after RVA ligation, indicating that flow is shunted from the RVA to the LVA. *, $P<0.05$ and **, $P<0.01$, pre- versus post-ligation. (**G-L**) In vivo imaging of diameter adaptation of RVA and LVA in control (G,I) and ligation (H,J) embryos shows progressive pruning of the RVA segment proximal to the ligation (L). The contralateral LVA in the ligation embryo now receives more flow and displays outward remodeling (K). *, $P<0.05$ and ***, $P<0.001$ versus ligation. VV, vitelline vein; p, proximal arteriole; d, distal arteriole. Scale bars: 0.62 mm in G,H; 1.25 mm in I,J.

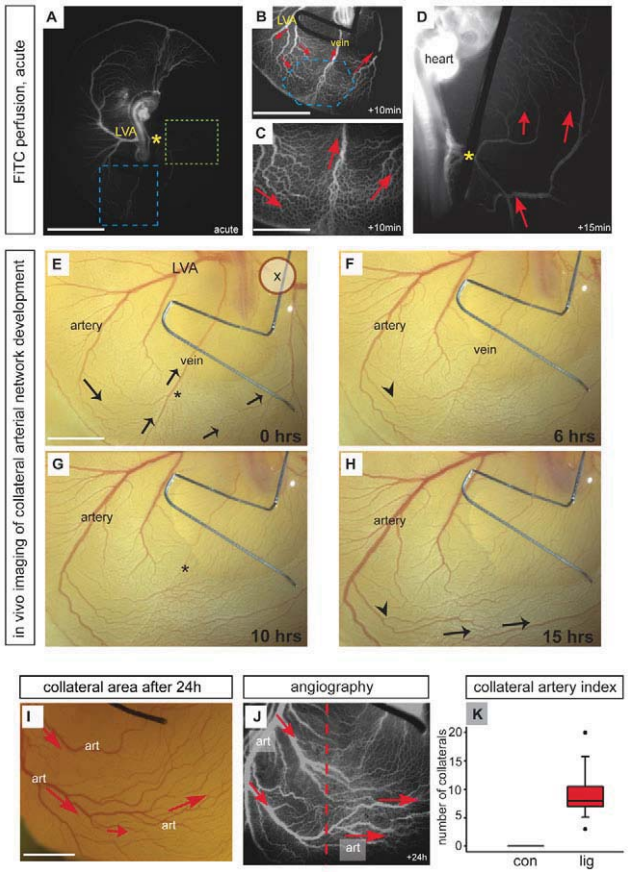

Fig. 4. Flow redistribution results in the formation of a collateral arterial network. (**A-D**) Acutely after ligation, FITC-dextran angiography indicates a perfusion deficit on the ligated side (A). Asterisk indicates site of RVA ligation. (B) Detail of blue box in A. (C) Detail of blue polygon in B. (D) Detail of green box in A. Within 10 minutes post-ligation (B,C), blood starts to flow from the posterior venous domain towards the ligated side via pre-existing RVA arteriolar channels (D). Red arrows indicate the flow direction. (**E-H**) Time-lapse imaging shows the rapid formation of an arterial network through the previously venous domain. Asterisk, pruned vein; arrowheads, growing artery; arrows, arterial flow direction; circled X, RVA occlusion site. (**I-K**) At 24 hours post-ligation, a significant number of perfused large-caliber arteries can be detected in ligation embryos (lig), but not in controls (con) (K). The vertical dashed line in J indicates the embryo/yolk sac midline. Scale bars: 4.9 mm in A; 1.8 mm in B; 3.1 mm in C; 3.6 mm E-H; 2.4 mm in I.

all animals investigated (Fig. 3I,J,L). By contrast, the arterial segment of the LVA showed increased diameter growth, which was already detectable 5 hours post-ligation (ligation, 289±30 µm; time-matched control, 252±22 µm; n=6 embryos, $P<0.05$; Fig. 3G,H,K) and was more pronounced after 24 hours (ligation, 381±22 µm; control, 299±12 µm; n=6 embryos, $P<0.05$; Fig. 3I,J,K). Thus, ligation of the RVA results in shunting of flow to the LVA network, causing outward remodeling in this area.

Redistribution of blood flow upon RVA ligation was further evaluated using FITC-dextran angiography (Fig. 4A-D). Acutely after ligation, the ligated right-hand side showed a clear perfusion deficit, whereas the LVA was well perfused (Fig. 4A). Within 10 minutes after ligation, blood flow was recruited to the right-hand side via retrograde perfusion of RVA arterioles in the posterior pole (Fig. 4B, detail in 4C). Thus, after ligation, blood now flows from the LVA network, through the posterior vitelline vein domain, into the pre-existing arterioles of the RVA arterial network back to the heart (Fig. 4D). In these RVA arterioles, pulsatility was reduced. RPSI values in RVA arterioles (n=5) dropped significantly from 11±0.5 second^{-1} (pre-ligation) to 1±0.25 second^{-1} (post-ligation), thus showing venous flow characteristics. Within 15 hours, the changes in flow distribution elicited a global change in arterial patterning (Fig. 4E-H). The LVA arterial network expanded towards the ligated right-hand side, with branches growing through the venous territory projecting towards the right-hand side of the embryo (Fig. 4E-H). Concomitantly, the posterior vitelline vein regressed. At 24 hours post-ligation, an elaborate collateral arterial network that restored flow to the occluded side was established in all embryos investigated (Fig. 4I-K). Collateral arteries were defined by a clear anatomical connection to the LVA, carrying an arterial flow profile and crossing

the embryo/yolk sac midline (Fig. 4I,J). In ligation embryos, the number of collateral arteries ranged from three to 20 (median=7, *n*=12 animals), whereas in control embryos such collateral arteries were never observed (*n*=14) (Fig. 4K). Ligation of the LVA also induced global changes in arterial patterning. In this case, arterial branches projected from the RVA, through the posterior pole towards the left side of the embryo, yielding a 'mirror' image of RVA ligation (see Fig. S5A in the supplementary material).

We next imaged the regression of the posterior vein in more detail using time-lapse intravital microscopy (see Movies 1-3 in the supplementary material). Before the ligation, flow from the LVA and RVA both drain into the vein (see Movie 1 in the supplementary material). Acutely after ligation, blood flow coming from the LVA was redistributed towards the vitelline vein and the arterial network on the ligated side using pre-existing vessel segments (see Movie 2 in the supplementary material). The flow direction in the RVA was reversed compared with pre-ligation. As a result of redirecting flow to the RVA, the amount of blood flowing to the vein decreased. This was associated with a progressive reduction in diameter and a subsequent pruning of the vein (see Movie 3 in the supplementary material).

To understand the vascular changes occurring at the capillary level, we imaged vascular casts of control and ligated embryos by scanning electron microscopy (Fig. 5A-H). We noted a striking induction of splitting angiogenesis [also referred to as intussusception (Djonov et al., 2000a; Djonov et al., 2000b)] in the ligation embryos. Splitting angiogenesis leads to an increase in vascular surface and in the number of segments, which involves the formation of trans-capillary pillars (Djonov et al., 2000a). Moreover, a special form of splitting angiogenesis [intussusceptive arborization (IAR)] leads to the separation of arterioles and venules from the capillary network (Djonov et al., 2000a; Djonov et al., 2000b). In IAR, pillars are formed in rows that demarcate the future large vessel in the capillary network. During subsequent steps, these pillars fuse, resulting in disconnection of the main vessel segment from the capillary plexus. We observed exactly this in the ligation embryos, but not in controls (compare capillaries in Fig. 5A,B with 5C,D). We detected numerous pillars at the level of the capillary plexus and distal parts of the expanding arterioles (Fig. 5C-H). Careful examination revealed that rows of pillars delineate the future territory of the arteriole (Fig. 5D,G). Subsequent fusion of these rows of pillars led to the separation of the feeding arteriole and its disconnection from the surrounding capillary network (Fig. 5F). Splitting angiogenesis was furthermore demonstrated in vivo by fluorescent labeling of endothelial cells (Fig. 5I,J) using *Sambucus* lectin (Pardanaud and Eichmann, 2006). The repetitive occurrence of this splitting process will successively give rise to a new generation of arterioles, molded out from the capillary network.

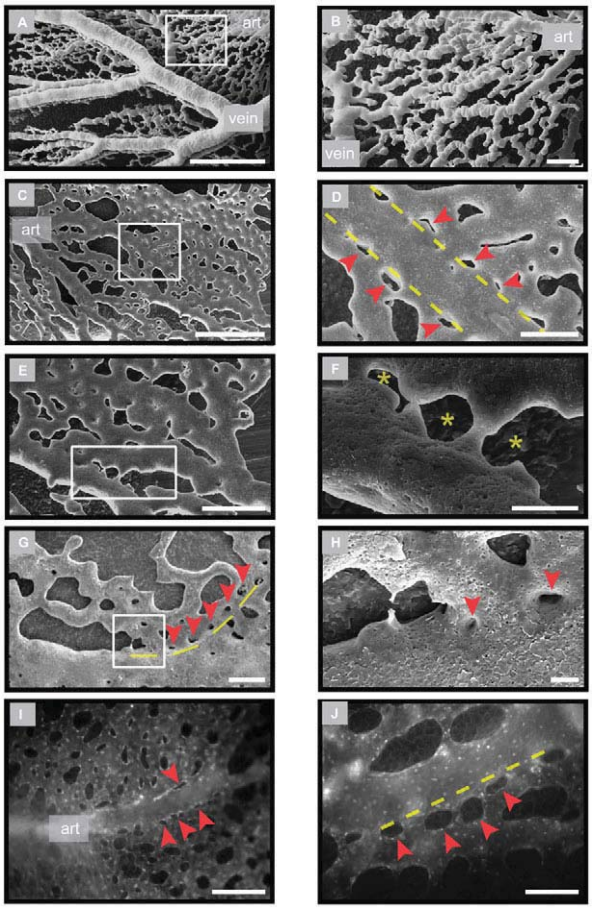

Fig. 5. Splitting angiogenesis (intussusception) in ligation embryos. (**A-H**) Scanning electron micrographs of vascular corrosion casts of control (A,B) and ligation (C-H) chicken embryos. (A) Low magnification of the normal vasculature. The boxed region is shown at higher magnification in B. Splitting angiogenesis is not apparent. (C) Micrograph of ligation embryo showing extensive pillar formation. (D) Magnification of the boxed region in C, showing rows of pillars (red arrowheads) delineating the future arteriolar segment (dashed line). (E,F) Overview (E) and detail of the boxed area (F) showing fusion of pillars leading to segregation of the capillaries (asterisks). (G,H) Another example showing the advanced splitting by pillars (arrowheads); rows of pillars align (dashed line) and subsequent fusion will lead to separation of the feed vessel from the surrounding capillary plexus. (**I**,**J**) Fluorescent labeling of endothelial cells in vivo shows pillar formation (arrowheads) in distal arterioles and the connected capillary network. art, artery. Scale bars: 500 μm in A,C; 200 μm in E; 100 μm in B,D,G; 50 μm in F; 20 μm in H; 30 μm in I,J.

Gja5 expression in developing yolk sac arteries

We performed in situ hybridizations to determine the expression of *Gja5* in the developing chicken embryo vasculature (Fig. 6). *Gja5* was expressed in the developing yolk sac arterial network, the aorta and in the developing arterioles of the limb bud (Fig. 6A-E). Expression in veins was not observed.

We next examined *Gja5* expression in the posterior pole of control and ligated embryos (Fig. 6F-I; see Fig. S5B in the supplementary material). At 20 hours post-ligation, all ligated embryos (*n*=12) showed a collateral arterial circulation crossing the venous territory and projecting towards the right-hand side of the embryo (Fig. 6H), which was not observed in controls (Fig. 6F). Using whole-mount in situ hybridization, we observed that the proportion of embryos showing *Gja5* expression in the venous territory (compare control Fig. 6G with ligation 6I) was significantly greater in ligated embryos than in time-matched controls (12/12 ligated embryos versus 0/8 control embryos with *Gja5* expression; $P<0.001$, *z*-test). Quantitative RT-PCR analysis (see Fig. S5B in the supplementary material) showed significantly increased expression of *Gja5* and *Dll4* in the collateral area (previously venous territory) of ligated embryos, confirming the arterial identity of these collateral vessels.

Ligation of the RVA resulted in perfusion of the RVA network with blood flow showing venous characteristics (see above). To determine whether this affected the arterial expression of *Gja5*, we compared

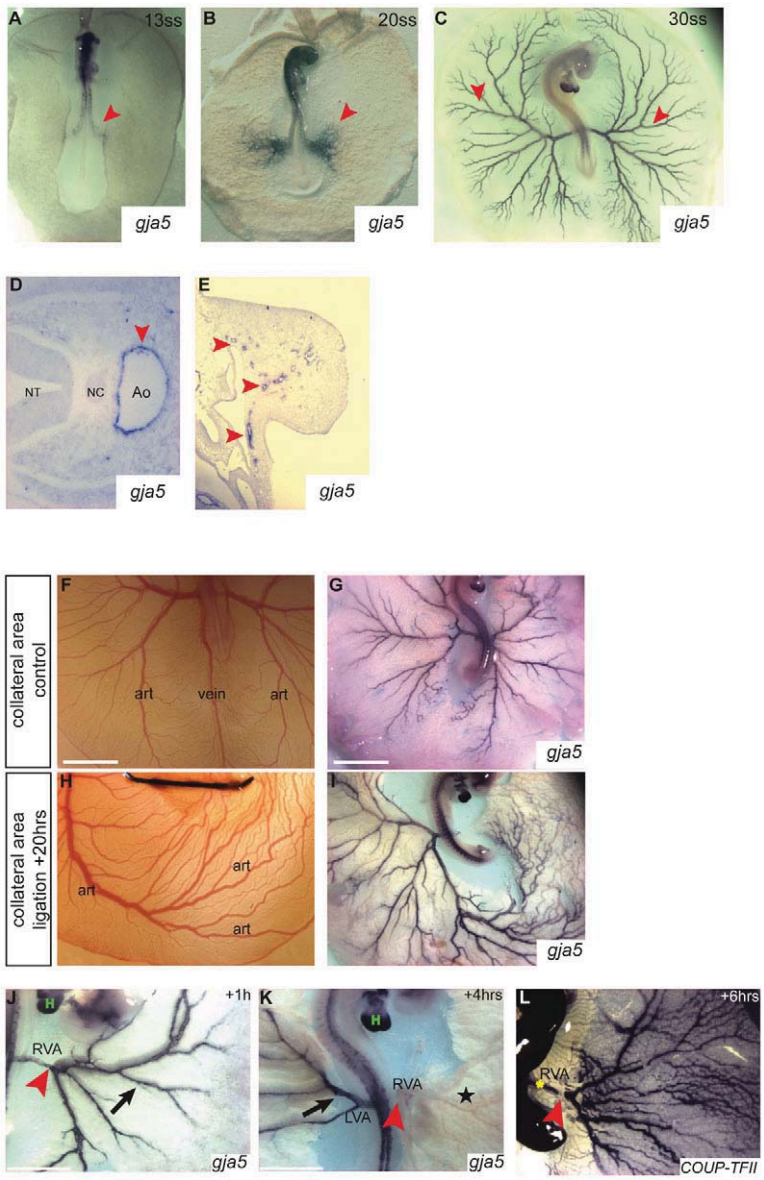

Fig. 6. Gja5 is expressed in arteries and regulated by flow. (**A-C**) Whole-mount in situ hybridization with a *Gja5* antisense riboprobe shows clear expression in the developing vitelline arterial network (arrowheads), but not in veins. (**D**,**E**) In situ hybridization on sections. *Gja5* is expressed in the aorta (D, arrowhead) and in the developing limb bud (E, arrowheads). (**F-I**) *Gja5* expression in normal (F,G) and ligation (H,I) embryos. Note the strong expression of *Gja5* in the collateral arterial network (I). (**J-L**) After ligation of the RVA, *Gja5* expression is still detectable after 1 hour (J, black arrow) but is absent after 4 hours (K, star). The LVA maintains *Gja5* expression (K, black arrow). The RVA arterioles now start to express the venous marker *COUP-TFII* (L). Note the expression of *COUP-TFII* in the RVA segment proximal to the ligation (L, yellow asterisk). Arrowhead in J-L indicates the ligation site. art, artery; NT, neural tube; NC, notochord. Scale bars: 2.8 mm in F,H; 2.3 mm in G,I; 1 mm in J; 1.6 mm in K.

Gja5 expression in the RVA network of ligated embryos at 1 and 4 hours post-ligation with time-matched unligated controls. At 1 hour (Fig. 6J), we observed no significant differences in the proportion of embryos with *Gja5* expression in the RVA tree of ligated embryos and their time-matched controls (8/10 ligated embryos versus 12/12 control embryos with *Gja5* expression; P=0.38, z-test). At 4 hours (Fig. 6K), the proportion of embryos with *Gja5* expression in the RVA tree was significantly lower in the ligated embryos than in the time-matched controls (0/7 ligated embryos versus 6/6 control embryos with *Gja5* expression; P<0.01, z-test). Thus, within 4 hours of ligation, the RVA network lost *Gja5* expression.

We next analyzed expression of the venous marker *COUP-TFII* (Fig. 6L). The proportion of embryos with *COUP-TFII* expression in the RVA was significantly greater in ligated embryos than in time-matched controls (6/7 ligated embryos versus 0/6 control embryos with *COUP-TFII* expression; P<0.05, z-test). Thus, in controls, *COUP-TFII* expression was always restricted to the vitelline veins, whereas ligated embryos expressed *COUP-TFII* in the RVA and vitelline veins.

Loss of Gja5 function is associated with reduced flow-driven arteriogenesis

To test whether Gja5 plays a functional role in flow-mediated adaptive remodeling of arteries, we investigated *Gja5* mutant mice using two established flow-driven arteriogenesis models: the hindlimb femoral artery occlusion (FAO) model (Fig. 7; see Fig. S7 in the supplementary material) and the mesenteric ligation model (see Fig. S8 in the supplementary material). In mice, Gja5 is expressed in arteries, both in embryo and adult (see Fig. S6 in the supplementary material).

In mice, ligation of the femoral artery results in the flow-driven formation of a collateral arterial network that bypasses the occlusion (see Fig. S7A in the supplementary material). The efficacy of this process can be assessed by repetitive non-invasive evaluation of hindlimb perfusion using laser Doppler perfusion imaging (LDF). Hindlimb perfusion did not differ among $Gja5^{-/-}$, $Gja5^{+/-}$ and wild-type (wt) mice prior to performing FAO (Fig. 7A). FAO reduced hindlimb perfusion in $Gja5^{-/-}$, $Gja5^{+/-}$ and wt mice to a similar extent (Fig. 7B). At 24 hours after FAO, hindlimb

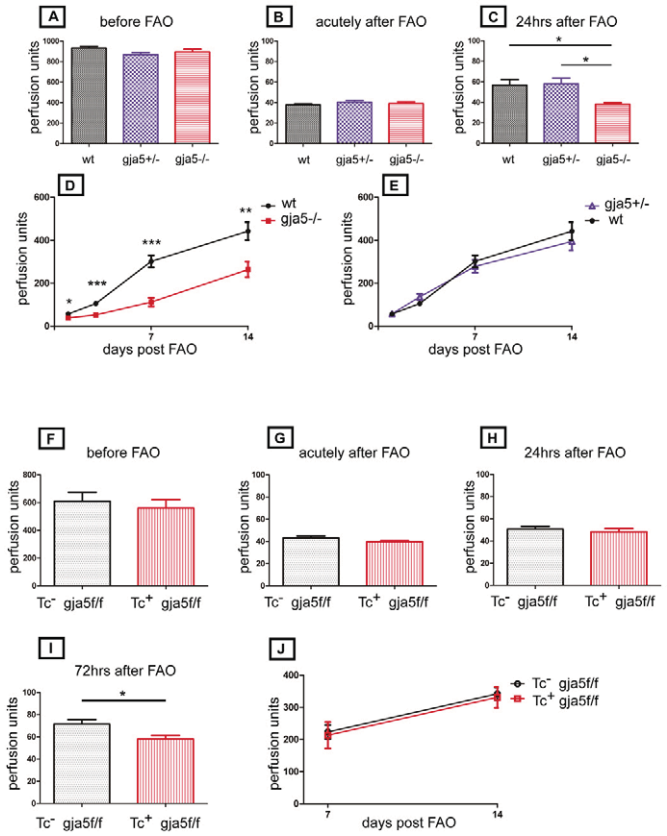

Fig. 7. Hindlimb perfusion after femoral artery occlusion in Gja5 loss-of-function models. (**A-C**) Hindlimb perfusion in wild-type (wt), *Gja5*$^{+/-}$ and *Gja5*$^{-/-}$ mice before femoral artery occlusion (FAO) (A), acutely after (B) and 24 hours after (C) occlusion. (**D**) Reduced perfusion in *Gja5*$^{-/-}$ mutants, until 14 days after FAO. (**E**) No differences are observed between *Gja5*$^{+/-}$ and wt. *n*=9 for wt and *Gja5*$^{+/-}$, *n*=11 for *Gja5*$^{-/-}$. (**F-J**) Effects of inducible endothelial-specific deletion of *Gja5* on hindlimb perfusion. At 72 hours a significant reduction was noted (I), but perfusion was restored to normal afterwards (J). Tc^{+} gja5f/f indicates inducible Cre^{+} *Gja5*$^{flox/flox}$ mice treated with tamoxifen. Tc^{-} gja5f/f indicates inducible Cre^{-} *Gja5*$^{flox/flox}$ mice treated with tamoxifen. *n*=8 for Tc^{-}, *n*=5 for Tc^{+}; *, *P*<0.05; **, *P*<0.01; ***, *P*<0.001.

perfusion was significantly lower (*P*<0.05) in *Gja5*$^{-/-}$ mice than in wt or *Gja5*$^{+/-}$ mice (Fig. 7C); *Gja5*$^{+/-}$ and wt mice were indistinguishable (Fig. 7E). Hindlimb perfusion remained significantly lower in *Gja5*$^{-/-}$ mice (Fig. 7D). Similar results were obtained upon microsphere perfusion assessment of the hindlimb (data not shown). FAO induced *Gja5* expression in the ischemic hindlimb to a similar extent in *Gja5*$^{+/-}$ and wt mice (see Fig. S9A in the supplementary material); expression was increased 4-fold 3 days after occlusion.

The efficacy of blood transport into the compromised hindlimb depends on the size and number of the collateral arteries. To quantify this, we imaged the morphology of the collateral arterial network in the hindlimb of *Gja5*$^{-/-}$and wt mice 7 days after FAO using microCT (see Fig. S7A-F in the supplementary material). Arterial collateral diameters were significantly smaller (*P*<0.05) in *Gja5*$^{-/-}$ (*n*=5) than in wt (*n*=4) mice (see Fig. S7G,H in the supplementary material). The total number of growing collaterals was smaller in *Gja5*$^{-/-}$ (3.8±0.37) than in wt (6.0±0.81) mice. To examine whether the reduced collateral diameters in *Gja5*$^{-/-}$ mice could arise from impaired flow-induced outward remodeling, we used the mesenteric ligation model (Loufrani et al., 2002) (see Fig. S8A in the supplementary material). Arteries from *Gja5*$^{-/-}$ mutant mice showed a reduced flow-driven outward remodeling response in this model (see Fig. S8B in the supplementary material). When blood flow was increased chronically in mesenteric resistance arteries, the resulting increase in diameter was significantly smaller in *Gja5*$^{-/-}$ than in wt mice.

Gja5 expressed in arterial endothelium can mediate vasodilatory responses. To investigate the involvement of this functional component we examined mice in which we deleted *Gja5* expression specifically from the endothelium prior to performing FAO (Fig. 7F-J). For this purpose, *Gja5*$^{flox/flox}$ mice were crossed with those bearing an endothelial-specific tamoxifen-inducible *Tie2 Cre* transgene, and treated with tamoxifen. Endothelial-specific deletion of *Gja5* (see Fig. S9B-D in the supplementary material) resulted in reduced hindlimb perfusion at 3 days after FAO (Fig. 7I). This corresponds to a time point at which Gja5 expression is high in the ischemic hindlimb in wt (see Fig. S9A in the supplementary material). Since our Cre-mediated recombination did not completely annihilate *Gja5* expression, residual Gja5 protein might have accounted for the relatively normal perfusion levels at other time points. However, collectively, our data support a model in which impaired flow-induced outward remodeling reduced collateral number and loss of vasodilation contributes to the perfusion deficit in *Gja5*$^{-/-}$ mutants.

DISCUSSION

We performed an extensive in vivo analysis of artery- and venous-specific characteristics related to flow, pressure and oxygen availability, and found that shear-related signals most likely contribute to the regulation of arterial identity and remodeling. We noted striking differences in flow pulsatility between arteries and veins. Theoretically, the steepness of the shear increase during early systole would be the strongest pulsatile signal available to endothelial cells. The best separation between arterial and venous vessels was indeed obtained by estimating this signal, i.e. the maximal positive change in shear rate relative to the time-averaged shear rate in the same vessel, termed RPSI (second^{-1}). Arteries have RPSI values exceeding 7.9 with 99% confidence, whereas the probability is only 5% for veins. Of course, these observations do not prove causality, and for RPSI to be physiologically relevant endothelial cells have to sense fluctuations in shear (Dai et al., 2004; Garcia-Cardena et al., 2001). In vivo, RPSI values above 7.9 correlated well with arterial marker expression. RVA ligation caused RPSI values in perfused vessels on the ligated side to drop from the arterial (above 7.9) to the venous (below 7.9) domain and were associated with loss of the arterial marker Gja5 and upregulation of the venous marker COUP-TFII. In addition, we show that the pressurized, non-perfused RVA segment proximal to the occlusion lost Gja5 and started to express COUP-TFII. This suggests that in this in vivo setting, pulsatility of flow/shear, not pressure, regulates arterial identity genes. Moreover, as arterial markers such as Gja5 are expressed in both low-oxygenated extra-embryonic vessels and well-oxygenated intra-embryonic vessels, it is also unlikely that oxygen per se is involved.

In normal embryos, yolk sac arteries and veins show relatively constant shear values, indicating that these vessels adapt their lumen size to the amount of flow carried. This was confirmed in the ligation model; arteries adapted their diameter rapidly (within hours) in response to changes in blood flow, consistent with the

concept of shear stress normalization to a given set point. Since acute vasomotor responses were not observed, these diameter changes are of a structural nature. In both arteries and veins, loss of perfusion resulted in rapid pruning. Anatomical properties of yolk sac vessels, including an incomplete vessel wall, may facilitate such rapid structural adaptation. Such unique plasticity of vessel shape and identity may be characteristic for the yolk sac vasculature and restricted to early development (Moyon et al., 2001).

In the ligation model, we observed that the expansion of the LVA tree through the venous domain was associated with the induction of splitting angiogenesis (Djonov et al., 2000a). Splitting angiogenesis is rapid compared with sprouting angiogenesis, and can give rise to new vessel segments within hours. It furthermore does not require a substantial change in endothelial cell number, as it involves the rearrangement of endothelial cells that are already in place. Indeed, in the ligation model, we did not detect any substantial changes in cell number. Essential for splitting angiogenesis is the formation of pillars and their fusion to allow segregation of the main vessel from the capillary bed (Djonov et al., 2000a; Djonov et al., 2000b). In line with this, we noted that the pillars were preferentially located lateral of the main thoroughfare channels, at the distal ends of the expanding arterioles. Collectively, flow-induced outward diameter remodeling and splitting angiogenesis facilitate the expansion of the LVA in the ligation model.

The role of Gja5 (connexin 40) in arteriogenesis

It is well established that neurogenesis and angiogenesis share common molecules and mediators (Carmeliet and Tessier-Lavigne, 2005), including the principle of electrical coupling involving gap junction proteins or connexins (Wagner, 2008). Connexins permit cross-talk between adjacent cells via the rapid exchange of ions and small metabolites. Arteries most notably express connexin 37 (Gja4) and connexin 40 (Gja5) (Wagner, 2008). *Gja5* and *Gja4* mutant mice are viable, but double-knockout mice die in utero and show angiogenic remodeling defects (Simon and McWhorter, 2002; Simon and McWhorter, 2003). Gja5 is preferentially expressed in endothelium, and mice deficient for Gja5 show impaired conduction of endothelium-dependent vasodilator responses along arterioles (de Wit et al., 2000). This conducted response can be evoked by local hypoxia, travel to upstream arterioles (Segal and Duling, 1986) and is believed to be crucial for the matching of oxygen delivery and tissue needs.

In the chicken embryo, Gja5 is expressed in the developing arterial network, starting at the onset of perfusion. In the ligation model, Gja5 expression followed the flow-induced arterial patterning. Moreover, exposing pre-existing RVAs to venous blood flow characteristics with low RPSI resulted in downregulation of *Gja5* expression. Compared with ephrin B2 and neuropilin 1 (le Noble et al., 2004), this downregulation was slow, suggesting that *Gja5* might be downstream of these genes.

The occlusion of a major supply artery can result in the formation of an endogenous arterial bypass circulation that restores perfusion to the compromised region (Schaper and Scholz, 2003), a process referred to as arteriogenesis. The efficacy of this process depends on the number of pre-existing collateral arterioles and their capacity to remodel outward into larger caliber arteries, as initiated by increased blood flow and shear stress (Eitenmuller et al., 2006). Gja5 was expressed in the femoral artery, and *Gja5* mutant mice showed reduced collateral blood flow after FAO. *Gja5* mutants had fewer and smaller collateral arterioles, which might well account for the perfusion deficit. Furthermore, mesenteric arteries from *Gja5* mutants chronically exposed to increased blood flow showed a reduced outward remodeling response, suggesting that Gja5 might act as a positive modulator of adaptation to flow. The reduction in the number of pre-existing collateral arterioles furthermore suggests that Gja5 might contribute to the formation of native collaterals. The mechanism that accounts for this observation (decreased collateral arteriole formation during embryogenesis, or enhanced pruning after birth) remains to be elucidated.

Acknowledgements

We thank Alexander Simon for connexin 40 mutant mice, Lucile Miquerol for connexin 40-EGFP knockin reporter mice, Michael Gotthardt for inducible *Tie2 Cre* mice, Takashi Mikawa for chicken Gja5 plasmid and Anja Zimmer for technical assistance. This study was supported by grants from the Helmholtz society, ECRC, The Netherlands Organization for Scientific Research (NWO) and CSB.

Competing interests statement

The authors declare no competing financial interests.

References

Adams, R. H., Wilkinson, G. A., Weiss, C., Diella, F., Gale, N. W., Deutsch, U., Risau, W. and Klein, R. (1999). Roles of ephrinB ligands and EphB receptors in cardiovascular development: demarcation of arterial/venous domains, vascular morphogenesis, and sprouting angiogenesis. *Genes Dev.* **13**, 295-306.

Buschmann, I. and Schaper, W. (1999). Arteriogenesis versus angiogenesis: two mechanisms of vessel growth. *News Physiol. Sci.* **14**, 121-125.

Carmeliet, P. (2000). Mechanisms of angiogenesis and arteriogenesis. *Nat. Med.* **6**, 389-395.

Carmeliet, P. and Tessier-Lavigne, M. (2005). Common mechanisms of nerve and blood vessel wiring. *Nature* **436**, 193-200.

Chadjichristos, C. E., Scheckenbach, K. E., van Veen, T. A., Richani Sarieddine, M. Z., de Wit, C., Yang, Z., Roth, I., Bacchetta, M., Viswambharan, H., Foglia, B. et al. (2010). Endothelial-specific deletion of connexin40 promotes atherosclerosis by increasing CD73-dependent leukocyte adhesion. *Circulation* **121**, 123-131.

Chalothorn, D., Zhang, H., Clayton, J. A., Thomas, S. A. and Faber, J. E. (2005). Catecholamines augment collateral vessel growth and angiogenesis in hindlimb ischemia. *Am. J. Physiol. Heart Circ. Physiol.* **289**, H947-H959.

Dai, G., Kaazempur-Mofrad, M. R., Natarajan, S., Zhang, Y., Vaughn, S., Blackman, B. R., Kamm, R. D., Garcia-Cardena, G. and Gimbrone, M. A., Jr (2004). Distinct endothelial phenotypes evoked by arterial waveforms derived from atherosclerosis-susceptible and -resistant regions of human vasculature. *Proc. Natl. Acad. Sci. USA* **101**, 14871-14876.

De Smet, F., Segura, I., De Bock, K., Hohensinner, P. J. and Carmeliet, P. (2009). Mechanisms of vessel branching: filopodia on endothelial tip cells lead the way. *Arterioscler. Thromb. Vasc. Biol.* **29**, 639-649.

de Wit, C., Roos, F., Bolz, S. S., Kirchhoff, S., Kruger, O., Willecke, K. and Pohl, U. (2000). Impaired conduction of vasodilation along arterioles in connexin40-deficient mice. *Circ. Res.* **86**, 649-655.

Djonov, V., Schmid, M., Tschanz, S. A. and Burri, P. H. (2000a). Intussusceptive angiogenesis: its role in embryonic vascular network formation. *Circ. Res.* **86**, 286-292.

Djonov, V. G., Galli, A. B. and Burri, P. H. (2000b). Intussusceptive arborization contributes to vascular tree formation in the chick chorio-allantoic membrane. *Anat. Embryol. (Berl.)* **202**, 347-357.

Duarte, A., Hirashima, M., Benedito, R., Trindade, A., Diniz, P., Bekman, E., Costa, L., Henrique, D. and Rossant, J. (2004). Dosage-sensitive requirement for mouse Dll4 in artery development. *Genes Dev.* **18**, 2474-2478.

Eitenmuller, I., Volger, O., Kluge, A., Troidl, K., Barancik, M., Cai, W. J., Heil, M., Pipp, F., Fischer, S., Horrevoets, A. J. et al. (2006). The range of adaptation by collateral vessels after femoral artery occlusion. *Circ. Res.* **99**, 656-662.

Forde, A., Constien, R., Grone, H. J., Hammerling, G. and Arnold, B. (2002). Temporal Cre-mediated recombination exclusively in endothelial cells using Tie2 regulatory elements. *Genesis* **33**, 191-197.

Fraisl, P., Mazzone, M., Schmidt, T. and Carmeliet, P. (2009). Regulation of angiogenesis by oxygen and metabolism. *Dev. Cell* **16**, 167-179.

Garcia-Cardena, G., Comander, J., Anderson, K. R., Blackman, B. R. and Gimbrone, M. A., Jr (2001). Biomechanical activation of vascular endothelium

as a determinant of its functional phenotype. *Proc. Natl. Acad. Sci. USA* **98**, 4478-4485.
Gerety, S. S. and Anderson, D. J. (2002). Cardiovascular ephrinB2 function is essential for embryonic angiogenesis. *Development* **129**, 1397-1410.
Gerety, S. S., Wang, H. U., Chen, Z. F. and Anderson, D. J. (1999). Symmetrical mutant phenotypes of the receptor EphB4 and its specific transmembrane ligand ephrin-B2 in cardiovascular development. *Mol. Cell* **4**, 403-414.
Gerhardt, H., Golding, M., Fruttiger, M., Ruhrberg, C., Lundkvist, A., Abramsson, A., Jeltsch, M., Mitchell, C., Alitalo, K., Shima, D. et al. (2003). VEGF guides angiogenic sprouting utilizing endothelial tip cell filopodia. *J. Cell Biol.* **161**, 1163-1177.
Girard, H. (1973). Arterial pressure in the chick embryo. *Am. J. Physiol.* **224**, 454-460.
Gustafsson, F., Mikkelsen, H. B., Arensbak, B., Thuneberg, L., Neve, S., Jensen, L. J. and Holstein-Rathlou, N. H. (2003). Expression of connexin 37, 40 and 43 in rat mesenteric arterioles and resistance arteries. *Histochem. Cell Biol.* **119**, 139-148.
Haefliger, J. A., Nicod, P. and Meda, P. (2004). Contribution of connexins to the function of the vascular wall. *Cardiovasc. Res.* **62**, 345-356.
Hellstrom, M., Phng, L. K., Hofmann, J. J., Wallgard, E., Coultas, L., Lindblom, P., Alva, J., Nilsson, A. K., Karlsson, L., Gaiano, N. et al. (2007). Dll4 signalling through Notch1 regulates formation of tip cells during angiogenesis. *Nature* **445**, 776-780.
Herzog, Y., Kalcheim, C., Kahane, N., Reshef, R. and Neufeld, G. (2001). Differential expression of neuropilin-1 and neuropilin-2 in arteries and veins. *Mech. Dev.* **109**, 115-119.
Hill, C. E., Rummery, N., Hickey, H. and Sandow, S. L. (2002). Heterogeneity in the distribution of vascular gap junctions and connexins: implications for function. *Clin. Exp. Pharmacol. Physiol.* **29**, 620-625.
Hoefer, I. E., van Royen, N., Rectenwald, J. E., Deindl, E., Hua, J., Jost, M., Grundmann, S., Voskuil, M., Ozaki, C. K., Piek, J. J. et al. (2004). Arteriogenesis proceeds via ICAM-1/Mac-1-mediated mechanisms. *Circ. Res.* **94**, 1179-1185.
Jones, E. A., Baron, M. H., Fraser, S. E. and Dickinson, M. E. (2004). Measuring hemodynamic changes during mammalian development. *Am. J. Physiol. Heart Circ. Physiol.* **287**, H1561-H1569.
Jones, E. A., le Noble, F. and Eichmann, A. (2006). What determines blood vessel structure? Genetic prespecification vs. hemodynamics. *Physiology (Bethesda)* **21**, 388-395.
Jones, E. A., Yuan, L., Breant, C., Watts, R. J. and Eichmann, A. (2008). Separating genetic and hemodynamic defects in neuropilin 1 knockout embryos. *Development* **135**, 2479-2488.
Krebs, L. T., Xue, Y., Norton, C. R., Shutter, J. R., Maguire, M., Sundberg, J. P., Gallahan, D., Closson, V., Kitajewski, J., Callahan, R. et al. (2000). Notch signaling is essential for vascular morphogenesis in mice. *Genes Dev.* **14**, 1343-1352.
Krebs, L. T., Shutter, J. R., Tanigaki, K., Honjo, T., Stark, K. L. and Gridley, T. (2004). Haploinsufficient lethality and formation of arteriovenous malformations in Notch pathway mutants. *Genes Dev.* **18**, 2469-2473.
Lawson, N. D., Scheer, N., Pham, V. N., Kim, C. H., Chitnis, A. B., Campos-Ortega, J. A. and Weinstein, B. M. (2001). Notch signaling is required for arterial-venous differentiation during embryonic vascular development. *Development* **128**, 3675-3683.
Lawson, N. D., Vogel, A. M. and Weinstein, B. M. (2002). sonic hedgehog and vascular endothelial growth factor act upstream of the Notch pathway during arterial endothelial differentiation. *Dev. Cell* **3**, 127-136.
le Noble, F., Moyon, D., Pardanaud, L., Yuan, L., Djonov, V., Matthijsen, R., Breant, C., Fleury, V. and Eichmann, A. (2004). Flow regulates arterial-venous differentiation in the chick embryo yolk sac. *Development* **131**, 361-375.
Limbourg, A., Ploom, M., Elligsen, D., Sorensen, I., Ziegelhoeffer, T., Gossler, A., Drexler, H. and Limbourg, F. P. (2007). Notch ligand Delta-like 1 is essential for postnatal arteriogenesis. *Circ. Res.* **100**, 363-371.
Lindert, J., Werner, J., Redlin, M., Kuppe, H., Habazettl, H. and Pries, A. R. (2002). OPS imaging of human microcirculation: a short technical report. *J. Vasc. Res.* **39**, 368-372.
Loufrani, L., Levy, B. I. and Henrion, D. (2002). Defect in microvascular adaptation to chronic changes in blood flow in mice lacking the gene encoding for dystrophin. *Circ. Res.* **91**, 1183-1189.
Lu, X., le Noble, F., Yuan, L., Jiang, Q., de Lafarge, B., Sugiyama, D., Bréant, C., Claes, F., De Smet, F., Thomas, J. L. et al. (2004). The Netrin receptor UNC5B mediates guidance events controlling morphogenesis of the vascular system. *Nature* **432**, 179-186.
Lucitti, J. L., Jones, E. A., Huang, C., Chen, J., Fraser, S. E. and Dickinson, M. E. (2007). Vascular remodeling of the mouse yolk sac requires hemodynamic force. *Development* **134**, 3317-3326.
Miquerol, L., Meysen, S., Mangoni, M., Bois, P., van Rijen, H. V., Abran, P., Jongsma, H., Nargeot, J. and Gros, D. (2004). Architectural and functional asymmetry of the His-Purkinje system of the murine heart. *Cardiovasc. Res.* **63**, 77-86.
Moyon, D., Pardanaud, L., Yuan, L., Breant, C. and Eichmann, A. (2001). Plasticity of endothelial cells during arterial-venous differentiation in the avian embryo. *Development* **128**, 3359-3370.
Mukouyama, Y. S., Shin, D., Britsch, S., Taniguchi, M. and Anderson, D. J. (2002). Sensory nerves determine the pattern of arterial differentiation and blood vessel branching in the skin. *Cell* **109**, 693-705.
Pardanaud, L. and Eichmann, A. (2006). Identification, emergence and mobilization of circulating endothelial cells or progenitors in the embryo. *Development* **133**, 2527-2537.
Pries, A. R., Secomb, T. W., Gessner, T., Sperandio, M. B., Gross, J. F. and Gaehtgens, P. (1994). Resistance to blood flow in microvessels in vivo. *Circ. Res.* **75**, 904-915.
Ruhrberg, C., Gerhardt, H., Golding, M., Watson, R., Ioannidou, S., Fujisawa, H., Betsholtz, C. and Shima, D. T. (2002). Spatially restricted patterning cues provided by heparin-binding VEGF-A control blood vessel branching morphogenesis. *Genes Dev.* **16**, 2684-2698.
Schaper, W. (2009). Collateral circulation: past and present. *Basic Res. Cardiol.* **104**, 5-21.
Schaper, W. and Scholz, D. (2003). Factors regulating arteriogenesis. *Arterioscler. Thromb. Vasc. Biol.* **23**, 1143-1151.
Schmidt, V. J., Wolfle, S. E., Boettcher, M. and de Wit, C. (2008). Gap junctions synchronize vascular tone within the microcirculation. *Pharmacol. Rep.* **60**, 68-74.
Segal, S. S. and Duling, B. R. (1986). Flow control among microvessels coordinated by intercellular conduction. *Science* **234**, 868-870.
Shutter, J. R., Scully, S., Fan, W., Richards, W. G., Kitajewski, J., Deblandre, G. A., Kintner, C. R. and Stark, K. L. (2000). Dll4, a novel Notch ligand expressed in arterial endothelium. *Genes Dev.* **14**, 1313-1318.
Simon, A. M. and McWhorter, A. R. (2002). Vascular abnormalities in mice lacking the endothelial gap junction proteins connexin37 and connexin40. *Dev. Biol.* **251**, 206-220.
Simon, A. M. and McWhorter, A. R. (2003). Role of connexin37 and connexin40 in vascular development. *Cell Commun. Adhes.* **10**, 379-385.
Simon, A. M., Goodenough, D. A. and Paul, D. L. (1998). Mice lacking connexin40 have cardiac conduction abnormalities characteristic of atrioventricular block and bundle branch block. *Curr. Biol.* **8**, 295-298.
Stalmans, I., Ng, Y. S., Rohan, R., Fruttiger, M., Bouche, A., Yuce, A., Fujisawa, H., Hermans, B., Shani, M., Jansen, S. et al. (2002). Arteriolar and venular patterning in retinas of mice selectively expressing VEGF isoforms. *J. Clin. Invest.* **109**, 327-336.
Styp-Rekowska, B., Disassa, N. M., Reglin, B., Ulm, L., Kuppe, H., Secomb, T. W. and Pries, A. R. (2007). An imaging spectroscopy approach for measurement of oxygen saturation and hematocrit during intravital microscopy. *Microcirculation* **14**, 207-221.
Swift, M. R. and Weinstein, B. M. (2009). Arterial-venous specification during development. *Circ. Res.* **104**, 576-588.
Takebayashi-Suzuki, K., Yanagisawa, M., Gourdie, R. G., Kanzawa, N. and Mikawa, T. (2000). In vivo induction of cardiac Purkinje fiber differentiation by coexpression of preproendothelin-1 and endothelin converting enzyme-1. *Development* **127**, 3523-3532.
Takeshita, K., Satoh, M., Ii, M., Silver, M., Limbourg, F. P., Mukai, Y., Rikitake, Y., Radtke, F., Gridley, T., Losordo, D. W. et al. (2007). Critical role of endothelial Notch1 signaling in postnatal angiogenesis. *Circ. Res.* **100**, 70-78.
Van Mierop, L. H. and Bertuch, C. J., Jr (1967). Development of arterial blood pressure in the chick embryo. *Am. J. Physiol.* **212**, 43-48.
Villa, N., Walker, L., Lindsell, C. E., Gasson, J., Iruela-Arispe, M. L. and Weinmaster, G. (2001). Vascular expression of Notch pathway receptors and ligands is restricted to arterial vessels. *Mech. Dev.* **108**, 161-164.
Wagner, C. (2008). Function of connexins in the renal circulation. *Kidney Int.* **73**, 547-555.
Wang, H. U., Chen, Z. F. and Anderson, D. J. (1998). Molecular distinction and angiogenic interaction between embryonic arteries and veins revealed by ephrin-B2 and its receptor Eph-B4. *Cell* **93**, 741-753.
You, L. R., Lin, F. J., Lee, C. T., DeMayo, F. J., Tsai, M. J. and Tsai, S. Y. (2005). Suppression of Notch signalling by the COUP-TFII transcription factor regulates vein identity. *Nature* **435**, 98-104.
Yuan, L., Moyon, D., Pardanaud, L., Breant, C., Karkkainen, M. J., Alitalo, K. and Eichmann, A. (2002). Abnormal lymphatic vessel development in neuropilin 2 mutant mice. *Development* **129**, 4797-4806.
Zhong, T. P., Childs, S., Leu, J. P. and Fishman, M. C. (2001). Gridlock signalling pathway fashions the first embryonic artery. *Nature* **414**, 216-220.